Journal of Hazardous Materials 436 (2022) 129263

Contents lists available at ScienceDirect

Journal of Hazardous Materials

journal homepage: www.elsevier.com/locate/jhazmat

Ultrasensitive and rapid colorimetric detection of urotropin boosted by effective electrostatic probing and non-covalent sampling

Wenfei Ren [a,b,1], Yuan Liu [a,1], Baiyi Zu [a,*], Jiguang Li [a,b], Da Lei [a], Tianshi Zhang [a,b], Xincun Dou [a,b,**]

[a] Xinjiang Key Laboratory of Explosives Safety Science, Xinjiang Technical Institute of Physics & Chemistry, Chinese Academy of Sciences, Urumqi 830011, China
[b] Center of Materials Science and Optoelectronics Engineering, University of Chinese Academy of Sciences, Beijing 100049, China

HIGHLIGHTS

- Modulation on non-covalent effect facilitated specific recognition to urotropin.
- Ultra-sensitivity promoted single urotropin particle detection *via* a facile mode.
- Highly efficient sampling guaranteed superior sensing effect on diverse surface.
- All-in-one strategy was applied to achieve rapid and on-site sensing in real scene.

GRAPHICAL ABSTRACT

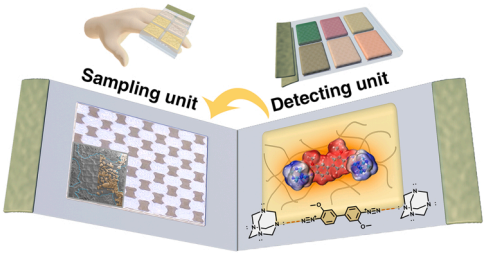

ARTICLE INFO

Editor: Lee Blaney

Keywords:
Hazardous chemicals
Efficient sampling
Chip-in-pocket
All-in-one design
Explosive

ABSTRACT

Leakage and contamination of hazardous chemical substances have been widely recognized as the critical issue in ensuring human health, maintaining environmental sustainability, and safeguarding public security. Urotropin as a crucial raw material in industrial holds a potential threat to aquatic/atmospheric environment with refractory degradation problem, hence, there remains a severe challenge to effectively and on-site monitor urotropin. Here, a general design with all-in-one strategy was presented, in which a highly integrated "pocket sensing chip" combining a sampling unit and a detecting unit together endows a rapid and ultrasensitive colorimetric detection without dead-zone towards urotropin. By loading fast blue B as sensing reagent in the detecting unit, a moderate and sensitive detection towards urotropin *via* electrostatic interaction was achieved with detection limits of 9 μM for liquid and 17.19 ng for particulates. Furthermore, an expandable sensing chip for the purpose of simultaneously screening on multi-target exhibited remarkable applicability for examining suspicious objects with all sorts of surface in real scenes, being unacted on environmental complexity. We expect this design would provide a universal strategy and the high referential value to propel the development of handy and portable sensing device to efficiently screen the environmental relevant critical substance on-site.

* Corresponding author.
** Corresponding author at: Xinjiang Key Laboratory of Explosives Safety Science, Xinjiang Technical Institute of Physics & Chemistry, Chinese Academy of Sciences, Urumqi 830011, China.
E-mail addresses: byzu@ms.xjb.ac.cn (B. Zu), xcdou@ms.xjb.ac.cn (X. Dou).
[1] contributed equally to this work. The manuscript was written through contributions of all authors.

https://doi.org/10.1016/j.jhazmat.2022.129263
Received 21 April 2022; Received in revised form 18 May 2022; Accepted 28 May 2022
Available online 1 June 2022

1. Introduction

Hazardous chemical substances have aroused huge threats to safe production, public security, and lead the global governments take their unusual presence, storage, and transport seriously (Germain and Knapp, 2009; Ke et al., 2022; Lee et al., 2020). Urotropin is often used as a key constituent in sterilant (Musher and Griffith, 1974), pesticide and solidifying agent (Taghdiri et al., 2013), beyond that, it is also used in high explosive manufacturing because of its readily availability including cyclonite (RDX) (Yi and Cai, 2008) and hexamethylene trioxide diamine (HMTD) (Dubnikova et al., 2005; Lock et al., 2012), which have become the powerful weapon in perpetrating terrorist attack. It is of utmost significance to strictly supervise its illegal storage and transporting to effectively lower the catastrophic threat of global terrorism and thoroughly investigate the explosion scenes. Moreover, urotropin is widely applied in industry, however, its trace leakage and pollution in aquatic and atmospheric environment could cause asthma and skin irritation (Cai et al., 2018; Gupta and Mittal, 2016; Taghdiri et al., 2013; Torphy, 1994), and the threshold limit value for occupational exposure is 3.0 mg/m^3 (Balasubramanian et al., 2003). Evidently, in support of the realistic application requirement, detecting urotropin has been trending away from the use of bulky, time-consuming laboratory instruments (Xu et al., 2017) and towards developing portable and rapid sensing strategies. In terms of the previously explored urotropin on-site detection methodologies, such as surface-enhanced Raman spectroscope (Cai et al., 2018), fluorescence (Zhang and Du, 2017) and colorimetry (Tininis et al., 2000), the less robust to against the environmental complexity as well as lack of the consideration in handling safety and practicability are still remarkable, which arouses the pressing need to develop accurate, anti-interferent, moderate and portable method to rapidly detect urotropin in real scenes which may involve complicated environmental settings.

Colorimetry is rapidly emerging as a preferable tool for conveniently recognizing and detecting different environmentally and biologically important analytes (Wang et al., 2021, 2018; Zheng et al., 2021), and when coupled with image analysis techniques and proper sampling, it has been demonstrated to provide remarkably high specificity and sensitivity, which is remarkably suitable for rapid on-site analysis (Lim et al., 2009; Matzeu et al., 2020; Wang et al., 2020a). Except the achievement of the specificity for the sensing reagent or the probe molecule towards target molecule, the signal response would be a decisive factor in developing highly sensitive on-site sensing method. For instance, the confinement effect was achieved by introducing Tween-20 in the sensing system which contributed to improving the colorimetric response on the surface and thus promoted the sensing performance (Liu et al., 2020). Furthermore, the portability of colorimetric sensors, especially for rapid on-site detection, was restricted due to the liquid state of the reagent which brings some inconvenience in carrying and storing, the alkalinity or acidity which causes varying degrees of damage to the surface of substances the analyte absorbing on, as well as complex operations bring the increase of training costs, and so on (Lin et al., 2021; Liu et al., 2018; Su et al., 2022). For solid analytes, sampling acts as another important part of detection in fluorescence, ion mobility spectroscopy (IMS) (Staymates et al., 2016) and colorimetry, and the sampling paper generally includes Nomex, muslin, acetate paper, or polytetrafluoroethylene-coated fiberglass weave (Forbes et al., 2020), which are mainly composed of directional or random fibers of raw pulp paper or non-woven fabric. The fiber structure of these sampling papers endows them with rough morphology and large specific surface area, thus enhancing the static friction force during sampling and improving the adsorption capacity of particles to a certain extent. Therefore, from the perspectives of improving the portability of colorimetric sensing and the sampling efficiency of solid particles both can be of great importance to facilitate the in-field detection performance, nonetheless only limited emphasis has been placed on in these fields. Is there any possibility to apply functional material (*e.g.*, hydrogel (Hu et al., 2020; Wang et al., 2020b)) and fully maximize its roles in loading the sensing reagent/probe and amplifying the response signal through keeping the colorimetric signal being observed simultaneously and minimizing the potential damage to the suspected surface such as skin, clothes, suitcase and so on? Meanwhile, would an ingenious design strategy contribute to a highly integrated sensing chip to further boost the sensing efficiency from both sampling and detection to minimize the operational complexity for wide-range real scenario application?

Herein, aiming at the pressing need of developing a mild sensing method to on-site detect trace urotropin in preventing its potential threat to surrounding environment, we proposed a highly integrated all-in-one strategy by combining the sampling unit and the detection unit together with a pocket size to achieve a high-efficiency on-site detection towards urotropin. Starting with the electrostatic interaction between the lone pair electrons of N of urotropin and the diazonium compound, fast blue B with strong electropositivity stood out from other diazonium salts to interact with urotropin and show a distinct colorimetric change. Series of desirable sensing performances were acquired and provided a solid foundation for equipping fast blue B within a hydrogel to form a detecting unit for particles determination. Moreover, by further loading other sensing reagent into the detecting unit, this sensing chip was extended as a multi-functional tool to coping with the practical need in routinely wide-range screening and exhibited great sensing capability to exam the potential hazardous chemicals in real scenarios. Therefore, this universal sensing strategy is expected to shine light on on-site critical substance monitoring in wider fields, such as noxious substances, explosives, and industrial emissions.

2. Materials and methods

2.1. Materials

Fast blue B salt ($C_{14}H_{12}Cl_2N_4O_2{\cdot}ZnCl_2$), acrylic acid (AA), N,N'-methylenebis(acrylamide) (MBAA), potassium persulfate ($K_2S_2O_8$, APS) and 1,5-cyclooctadiene were obtained from Sigma-Aldrich (Shanghai, China). Potassium tetrachloroplatinate (II) (K_2PtCl_4), 2,2':6',2''-terpyridine, ethyl acetate, sodium nitrate ($NaNO_3$), 4-(Dimethylamino) cinnamaldehyde (P-DMAC), sodium perchlorate ($NaClO_4$), sodium sulphate (Na_2SO_4), sodium carbonate (Na_2CO_3), dimethyl sulfoxide (DMSO), N,N-dimethylformamide (DMF), 2-methoxyethanol, 1-naphthol, 2,3-dihydroxynaphthalene, and polyvinyl alcohol (PVA1799, polymerization degree: 1750 ± 50, alcoholysis degree: 98.0–99.0%) were purchased from Aladdin (Shanghai, China). Polydimethylsiloxane (PDMS) Sylgard 184 was purchased from Dow Corning (Michigan, US). 4-diazo-3-methoxydiphenylamine was obtained from Macklin (Shanghai, China). PSA (SP7533) was purchased from 3 M (Shanghai, China). The other chemicals used in this study were purchased from Sinopharm Chemical Reagent Co., Ltd. All chemicals were analytical-reagent grade and used directly without further purification. Ultrapure deionized water (18.2 MΩ) was used to prepare the hydrogel.

2.2. General characterizations

Ultraviolet-visible (UV–vis) spectra were recorded on a portable optical detector, which was built by a grating spectrometer (Ocean Optics, Maya 2000 Pro), a cuvette holder (Ocean Hood, CUV-10–4-WAY) as well as a light source consisting of deuterium lamp and halogen lamp (Ocean Hood, DH2000). Optical transmittance spectra were recorded on a Hitachi U3900 UV–vis spectrophotometer and a self-built portable spectrometer. Field-emission scanning electron microscopy (FE-SEM, JEOL JSM-7610 F Plus) was used for morphology characterization with a voltage of 4.0–6.0 kV. Elemental analysis was performed by an Energy-Dispersive Spectroscopy System (EDS, OXFORD X-Max 50) equipped on the FE-SEM. Attenuated total reflection Flourier transformed infrared (ATR-FTIR) spectra were obtained using a PerkinElmer Frontier with a universal ATR sampling accessory from PerkinElmer.

The digital photographs were captured by an industrial camera (Vision Datum Mars 5000S-20gc). The reaction-diffusion process of urotropin particles with different masses on the fast blue B-PAA hydrogel sensor were filmed by a video camera (Imavision, MER-2000–5GM/C-P) with a minimum resolution of 1.2 μm × 1.2 μm.

2.3. Preparation of fast blue B solution

14.3 mg fast blue B was added in 30 mL 2-methoxyethanol with a magnetic stirring of 20 min to form a homogeneous solution, followed by a filtration with a 0.22 μm syringe filter to remove the insoluble impurities. Thus, 1 mM fast blue B reagent was obtained and stored in dark for future usage of detecting urotropin solution.

2.4. Preparation of the polyacrylic acid (PAA) hydrogel based detecting unit

PAA hydrogel was prepared according to a previously reported literature with slight modification (Jing et al., 2018). The PAA aqueous prehydrogel was firstly prepared by dissolving 1.4 g AA, 20 mg MBAA, and 200 μL 25 g L^{-1} APS (in ultrapure deionized water) in 10 mL ultrapure deionized water consecutively with magnetic stirring for 10 min. Next, the PAA aqueous prehydrogel was poured into an airtight glass mold with a customized size followed by heating the mold at 65 °C for 6 h. After that, the PAA hydrogel was soaked in the ultrapure deionized water for storage. The water content (WC) of the as-prepared PAA hydrogel is 99.79%, calculated according to the reported references (Hu et al., 2020; Louf et al., 2021; Su et al., 2021). To obtain the hydrogel detecting unit, the as-prepared PAA hydrogel (10 × 10 × 1 mm) was immersed in 20 mL 2 mM fast blue B salt solution for 2 h at room temperature, thus, the fast blue B salt incorporated hydrogel detecting unit was acquired.

2.5. Construction of the sampling unit and pocket sensing chip

By applying screen-printing, the pressure-sensitive adhesive (PSA) was patterned onto the filter paper as the sampling unit. A transparent polyethylene glycol terephthalate polymer membrane was applied as the main substrate to integrate the detecting unit with the sampling unit together, for which the PSA was also applied to adhere the back side of the sampling unit onto the substrate while the detecting unit was fixed onto the substrate *via* its own adhesion.

In terms of the construction of the six-in-one sensing chip array, PDMS was employed to fabricate the barrier to separate each two adjacent sensing units by pouring a mixture of the PDMS Sylgard 184 base and curing agents (10:1 by weight) into a prepared resin mold followed by a heating step at 70 °C for 5 h. After washing the PDMS barrier with ethanol for several times, each detecting unit was fixed at an individual area.

2.6. Calculation method

An optimization strategy combined a global semi-empirical quantum mechanical search and density functional theory (DFT) was adopted to determine the most stable structures of urotropin, fast red B, 4-diazo-3-methoxydiphenylamine, fast blue B as well as the complex of urotropin and fast blue B by the Gaussian 09 (Frisch et al., 2016). All of the geometries were fully optimized using the B3LYP (Stephens et al., 1994) with Grimme's DFT-D3(BJ) (Grimme et al., 2011) empirical dispersion correction abbreviated as B3LYP-D3(BJ) with the def2-SVP (Weigend, 2006; Weigend and Ahlrichs, 2005) basis set. A larger basis set def2-TZVP (Weigend, 2006; Weigend and Ahlrichs, 2005) with CAM-B3LYP-D3(BJ) (Yanai et al., 2004) was adopted to obtain higher quality wave functions and were further used for the minimum electrostatic potential (ESP) (Murray and Politzer, 1998) and independent gradient model (IGM) (Lefebvre et al., 2017) analysis. A further frequency calculation at the same theory level was also performed at the optimized geometries to ensure that the located minimum points have all positive frequencies. In order to simulate the absorption condition, the time dependent density functional theory (TD-DFT) (Scalmani et al., 2006) calculations were carried out to obtain the vertical excitation energies for 30 lowest singlet transitions at the CAM-B3LYP/def2-TZVP level. The convolution of the spectrum was obtained using a gaussian function with a full width at half maximum (FWHM) of 0.3 eV. The polarizable continuum model (PCM) (Miertus et al., 1981; Pascualahuir et al., 1994) was employed to take into account the effect of 2-methoxyethanol solvent. SAPT2 + /aug-cc-pVDZ level was employed in our analysis. Symmetry-adapted perturbation theory (SAPT) (Parker et al., 2014) was carried by PSI4 1.5 code (Parrish et al., 2017). All above the wave function analyses were conducted by using Multiwfn software (Lu and Chen, 2012b) and the VMD 1.9.3 program (Humphrey et al., 1996) was used to plot the graph. In order to elucidate the interaction between the fast blue B and urotropin from an energy perspective, we conducted symmetry-adapted perturbation theory (SAPT) analysis.

3. Result and discussion

3.1. Overview of the all-in-one sensing strategy

Considering that the universal adaptability and the well-acceptable compliance are great of significance for efficiently wide-range screening in real scenarios, the sampling, detecting, and signal output were integrated as all-in-one scheme based on an elaborately design (Fig. 1). Starting with the finely selection of the sensing reagent with couple of diazonium salts whose N^+ enables a high affinity towards the lone pair electrons of N of urotropin, the polyacrylic acid (PAA) hydrogel was employed as the basic sensing substrate to load the optimal diazonium salt based on hydrogen interaction as the detecting unit. With the aid of the screen-printing, the pressure-sensitive adhesive (PSA) was attached onto the filter paper to be manufactured as the sampling unit which inherently holds the multi-interaction with the texture of the potential suspect substances. A polymer membrane was applied as the main substrate to integrate the detecting unit with the sampling unit together and extra provides an omnidirectional physical touch due to its soft and flexible character and an intuitive observation of colorimetric signal from its transparent morphology. Generally, this portable sensing chip with an all-in-one scheme can be adopted universally *via* inversely folding and wrapping the chip around the hand of the operator to ensure the sampling unit face down to the potential suspect substance and by gently pressing to adhere the particles on the object surface. Afterwards, the detecting unit side was folded 360 degrees to merge with the sampling unit side. In detail, the particles fully contact with the sensing reagent which is confined into PAA hydrogel network, and then the sensing outcome could be acquired

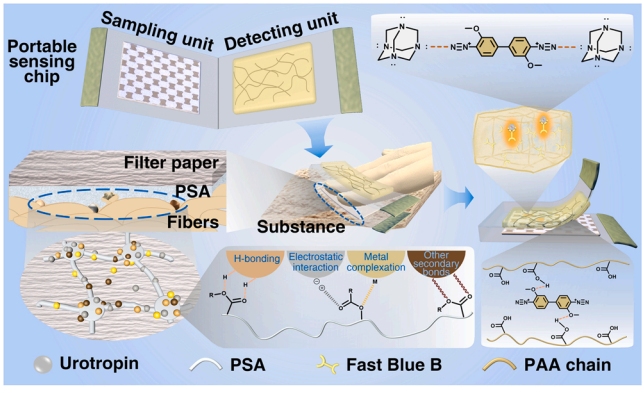

Fig. 1. Schematic illustration of the highly integrated sensing chip and the proposed mechanism for sampling and detecting.

straightforward and immediately *via* naked-eye observing the coloring on detecting unit side through the transparent polymer substrate.

3.2. Electrophilic effect of diazonium enabled colorimetric sensing towards urotropin

By means of density functional theory (DFT), the interaction mechanism between urotropin with diazonium as well as the corresponding optical property were systematically studied. It was found that urotropin enables an electrostatic potential (ESP) at N atoms with a value around − 28.6 kcal/mol, which were inclined to strongly combine with the electrophilic substance *via* electrostatic interaction (Fig. 2a) (Lu and Chen, 2012a; Murray and Politzer, 1998). Thus, couple of diazoniums due to their electrophilic character were examined with ESP profile, showing that fast blue B hold the maximal ESP at two diazonium groups (176.83 and 160.69 kcal/mol) while fast red B (147.93 kcal/mol) and 4-diazo-3-methoxydiphenylamine (103.10 kcal/mol) only carry one diazonium group and exhibited relatively weaker ESP. The possible

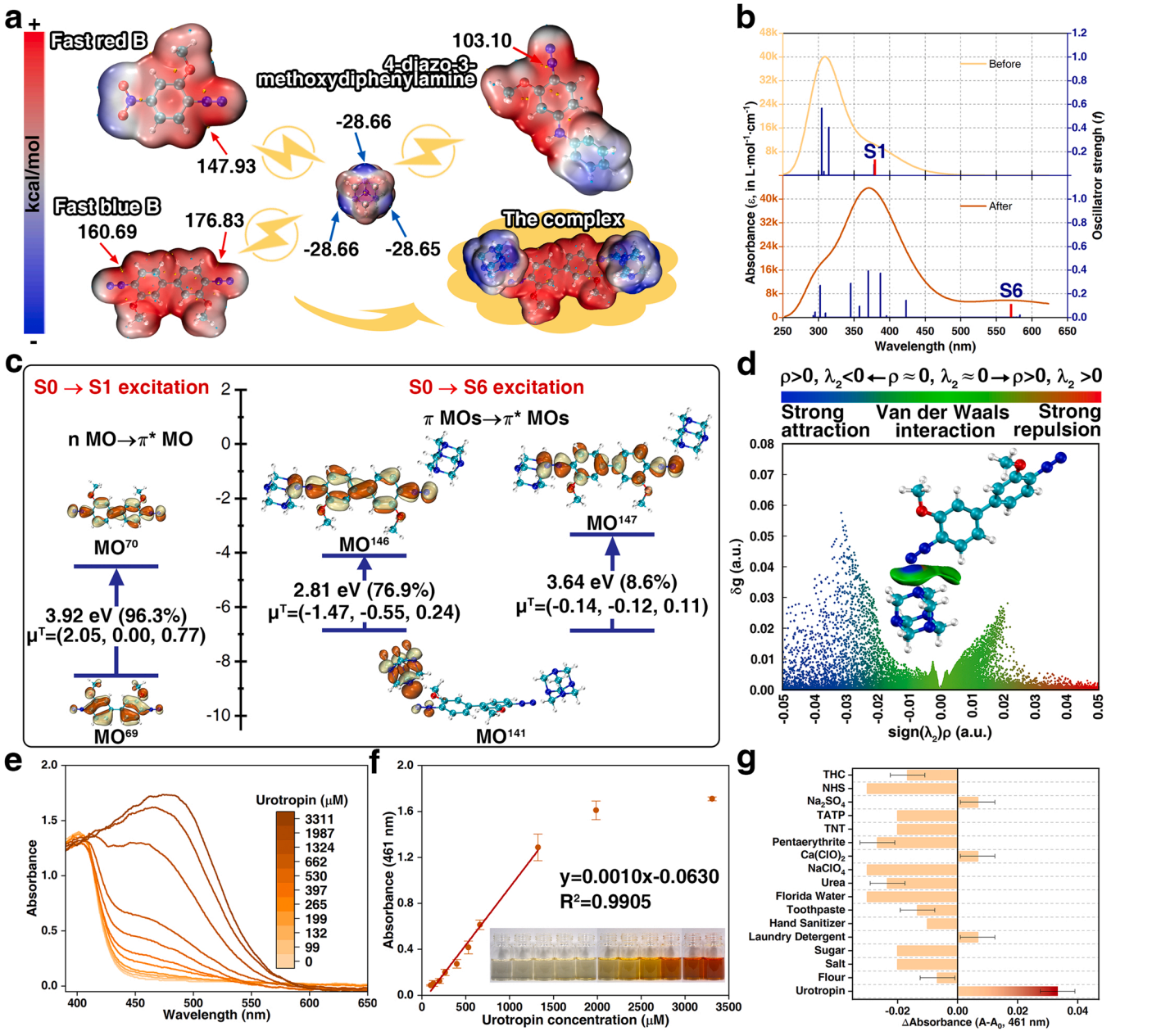

Fig. 2. (a) ESP-mapped molecular van der Waals (vdW) surface of urotropin, fast red B, 4-diazo-3-methoxydiphenylamine, fast blue B as well as the complex of urotropin and fast blue B, surface maximal and minimum of ESP presented in gold and cyan dots, respectively. (b) Simulated ultraviolet-visible (UV–vis) absorption spectra (curve) before and after interacting with urotropin by the full width at half-maximum of 0.3 eV from the broadened oscillator strength (spikes). (c) Dominant contributions of molecular orbital (MO) transitions in the process of interaction: S0→S1 excitation (isovalue = 0.05) and S0 → S6 excitation (isovalue = 0.05). Light yellow and dark orange regions denote the positive and negative orbital phases, respectively. The numbers of the outside and the inside of the parentheses denote the energy gaps of orbital (in eV) and the contributions of the transition to corresponding excitation, respectively. The value of μ^T stands for contribution of each orbital transition to transition dipole moment (in a.u.). (d) Independent gradient model (IGM) scatter graph and isosurface (value=0.01 a.u.) of the non-covalent interactions between urotropin and fast blue B. (e) UV–vis absorption spectra measured at 20 s while the urotropin solution with a varied concentration from 0 to 3311 μM was added in fast blue B solution. (f) The absorption intensities at 461 nm with a linearly fitted curve and the corresponding images. (g) Selectivity study of fast blue B solution towards series of urotropin solution with the presence of different interferents.

explanation could be that electron property of the surrounding groups of the diazonium group differs from each other, for example, the $-NO_2$ in fast red B shows a certain electron withdrawing effect to make its diazonium group more positive, while there is no electron withdrawing group within 4-diazo-3-methoxydiphenylamine leading to its diazonium group less electron-positivity. In terms of fast blue B, two diazonium groups express relatively stronger electron withdrawing interaction towards each other, empowering the electropositivity for both diazonium groups were lifted significantly and fast blue B potentially have better affinity towards urotropin due to more diazonium groups. Hence, the UV–vis absorption spectra and the corresponding images (Fig. S1) were applied to experimentally verify the above theoretical deduction under the optimized condition, in which slight color change can be seen for fast red B after interacting with urotropin while no observable color changed and spectrum altered in the case of 4-diazo-3-methoxydiphenylamine and urotropin. There was an apparent color change for fast blue B from light yellow to golden before and after interacting with urotropin and a new peak at 461 nm found in UV–vis absorption spectrum, indicating a strong interaction occurred (Fig. 2b). Time-dependent Density Functional Theory (TD-DFT) (Scalmani et al., 2006) method was adopted to calculate the excitation energies and the oscillator strengths (*f*) of fast blue B before and after interacting with urotropin, the calculational *f* and excitation energy of the specific excited states were used to simulate the UV–vis absorption spectra considering the solvent environment. Comparing to the main absorption peaks of fast blue B located at around 320 nm plus a shoulder peak at 375 nm (f=0.13), the main absorption peak shifted to 370 nm and a new peak appeared at around 570 nm (f=0.11) after interacting with urotropin.

To further investigate the alteration of these absorption peaks, from the molecular orbital (MO) analysis of the excited states, the shoulder peak at 375 nm was mainly ascribed to S0→S1 from the critical MO^{69}→MO^{70} transition (Fig. 2c), which corresponds to the n→p * excitation with a fraction of 96.3% of the total excitation energy and a quite large transition dipole moments (μ^T =(2.05, 0.00, 0.77)). After the addition of urotropin, the new appeared peak at around 570 nm was from the S0→S6 induced by MO^{141}→MO^{146} and MO^{141}→MO^{147} transitions with fractions of 76.9% and 8.6% of the total excitation energy and the μ^T values of (−1.47, −0.55, 0.24) and (−0.14, −0.12, 0.11), respectively. This result suggests that the excitation of the fast blue B altered from n→p * to p→p * due to the existence of urotropin, which was embodied as the decreased energy gaps from 3.92 eV to 2.81 eV and 3.64 eV, indicating that the absorption peak started to shift into the visible light region. Furthermore, it is considered that the diazonium of fast blue B and the N atoms in urotropin could be bound in the form of electrostatic interaction (Table S1), this strong intermolecular attraction was verified by the discrete dots in the scatter graph of similar patterns with spikes around the negative $sign(\lambda_2)\rho$ (−0.03) and the δ values close to 0.06 obtained by the independent gradient model (Fig. 2d) (Lefebvre et al., 2017).

As expected, an apparent enhancement of the absorption at 461 nm could be observed in the UV–vis spectra with the addition of different concentrations of urotropin (99–3311 μM, Fig. 2e), this absorption enhancement suggested a progressively deepened color trend in the optical images from light yellow, bright yellow, golden to orange (Fig. 2 f). The correlation between the enhanced absorption and the increasing urotropin was established and the fitted curve exhibits a good linearity when the urotropin concentration varied from 99 to1324 μM, accordingly, the limit of detection (LOD) was further obtained as 9 μM which was defined as LOD = $3\sigma/k$ (k represents the slope of the linear fragment of the fitted calibration curve with a value of 0.0010, and σ stands for the standard deviation of noise with a value of 0.0030. Furthermore, a time-dependent observation of the coloring response towards series of urotropin shows an instantly visualized coloring and the absorption at 461 nm fluctuated within 0.096 during 60 s (Fig. S2 and Table S2). When the observation lasted for longer time, it is noted that the color started to fade after 10 min and faded significantly after 20 min (Supplementary video 1), which could be confirmed by UV–vis absorption spectra as well (Fig. S3). It illustrates that the colorimetric sensing signal is quite reliable for a certain period which is long enough to make a judgment for on-site detection.

Supplementary material related to this article can be found online at doi:10.1016/j.jhazmat.2022.129263.

To further investigate the specificity of fast blue B salt toward urotropin, the common daily necessities (including flour, salt, sugar, laundry detergent, hand sanitizer, toothpaste, Florida water), the hazardous chemicals/explosives as well as structural analogues, were selected as potential interferents. Upon the addition of the 15 mM urotropin, the absorbance at 461 nm elevated significantly, while various analytes with 3.3 times higher concentration (50 mM) were added into fast blue B, the absorption at 461 nm decreased at different extent except laundry detergent, $Ca(ClO)_2$ and Na_2SO_4 which three showed neglectable increase (Fig. 2 g and S4a). The coloring change also shows that only the addition of urotropin induced the emergence of a bright yellow from light yellow, this well verifies that the fast blue B possesses desirable specificity to discriminate urotropin with other potential interferents (Fig. S4b). The reasonable explanation could be that N with lone pair electrons (*e.g.*, urotropin) shows stronger electrostatic interaction with fast blue B. In terms of the structural analogues, N-hydroxy succinimide (NHS) and urea which also contain N atom but equip with the positive ESP (Fig. S5), would not be apt to form electrostatic interaction with fast blue B embodied as no obvious coloring response after mixing with fast blue B. It should be noted that this fast blue B reagent is also inert to tetrahydrocannabinol (THC), which is different from the common magenta coloring process used in forensic analysis with the presence of NaOH (Bordin et al., 2012; Kanter et al., 1982) demonstrating the excellent selectivity of the present design.

3.3. Sensing of floating urotropin particulates

The sensing reagent loaded hydrogel substrate can be applied as a promising candidate to visually detect the particulate matter in real scenes, such as on the surface of clothes, as it could be bent into large angle for omnidirectional sampling. Among various available hydrogel matrixes (Li et al., 2019; Tan and Park, 2021), the chemically cross-linked polyacrylic acid (PAA) hydrogel was determined as a substrate in this work, because of its highly transparent and colorless morphology in the visible region (≥99%) as well as electrical-neutrality property to benefit for stabilizing the loaded fast blue B solution (Xu et al., 2018) (Fig. 3a and S6). As observed in SEM characterization, the PAA hydrogel substrate exhibited a porous morphology with an even pore size distribution, ranging from 20 to 50 μm (Fig. S7), which affords the three-dimensional skeleton and plenty of cavities to carry large amount of fast blue B molecules. After loading, the hydrogel showed slightly beige but transparent whose transmittance was maintained as 80% at 420 nm, providing a desirable background color to be differentiated with the characteristic color of the interaction between fast blue B towards urotropin. The success of incorporation of fast blue B was also demonstrated based on Flourier trans formed infrared (FTIR) spectroscopy analysis as no chemical damage to the PAA hydrogel occurred, being embodied as the existence of the characteristic peaks of the hydrogel skeleton (carboxyl at 2933 cm^{-1}, carbonyl at 1700 cm^{-1}) during the entire process (Fig. S8). Comparing with the detection towards urotropin solution, the absorbance around 461 nm of the fast blue B-PAA hydrogel sensor also increased obviously after detecting urotropin particles, likewise, its color changed into bright yellow, aligning well with the color change in detecting urotropin solution (Fig. 3b). Moreover, by making the small particles of 18 potential co-existing interferents float down to the hydrogel detecting unit (Fig. 3c), it shows that only the urotropin particles led to a bright yellow, flour and TNT particles caused distinguishable light orange, and all others were inert to the hydrogel detecting unit. By further extracting the Hue-Saturation (HS) color values of 20 points at the surrounding area of

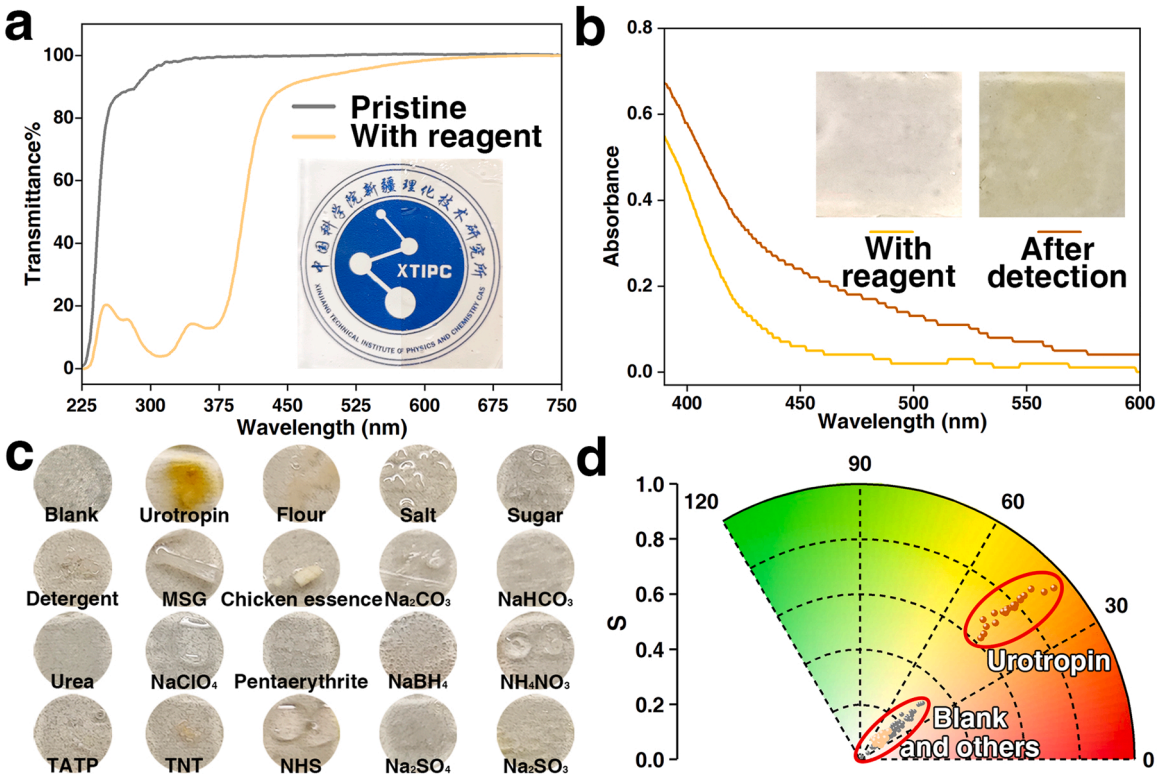

Fig. 3. (a) Optical transmittance of the prepared pristine PAA hydrogel (gray) and the fast blue B loaded PAA hydrogel (yellow). (b) UV–vis spectra and the corresponding images of the fast blue B-PAA hydrogel detecting unit before and after detection of urotropin particles. (c) Optical images of the anti-interference characterization of the fast blue B-PAA hydrogel detecting unit to 18 interferents particles. (d) Data coordinates of the urotropin particles and interferents particles in the Hue-Saturation (HS) color system.

each particle, it can be found that the coordinate positions of urotropin particles formed a separate cluster and were far away from those of the interference particles. These results strongly illustrate that the hydrogel detecting unit holds good specificity towards urotropin particulates and the hydrogel substrate did not influence this specific recognition at all (Fig. 3d).

3.4. Signal amplification facilitated single urotropin particulate detection

Except the role as a carrier to eliminate the concern of the operational safety aroused by sensing reagent itself, the hydrogel skeleton offers a signal amplification function which could enlarge the edge of the particulate falling onto the hydrogel surface rather than the original particle size. Hence, when urotropin particulates were floating nearby and part of them physically fell onto the surface of the fast blue B-PAA

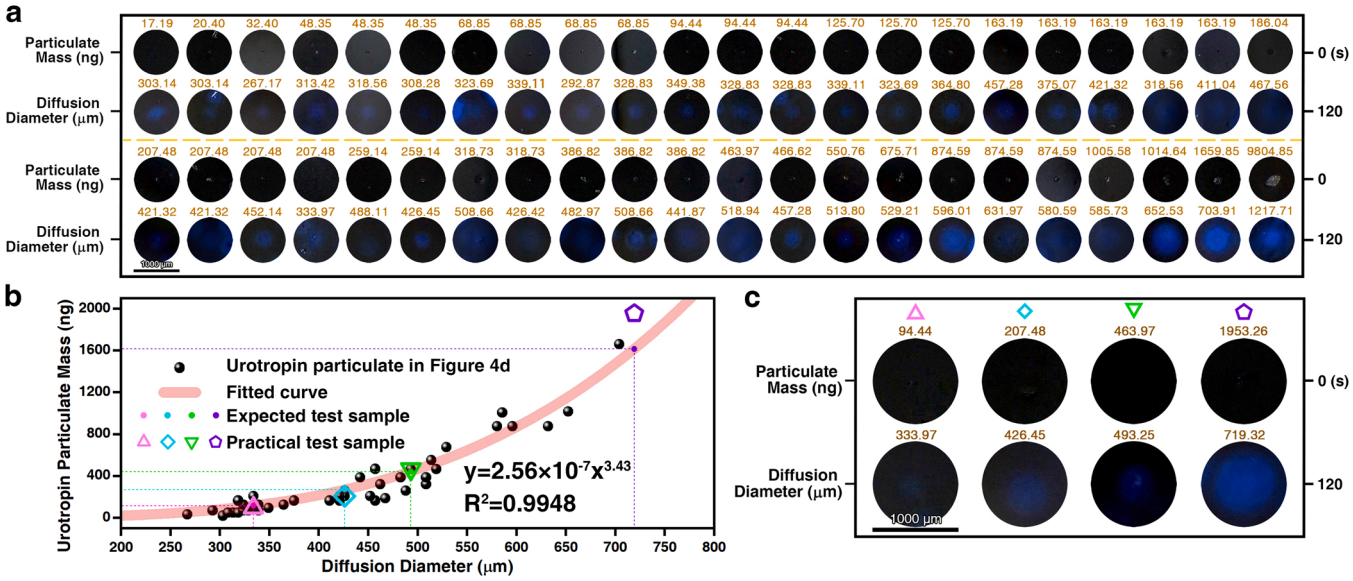

Fig. 4. (a) Images for each particulate fell onto the hydrogel sensor at 0 s and 120 s (n = 44). (b) Correlation curve between diffusion diameter at 120 s and the calculated particle mass. (c) Diffusion images of the four particulates chosen as the test sample.

hydrogel sensor, subsequently diffused into the liquidous micro-environment enclosed with the hydrogel skeleton and immediately reacted with the free-state fast blue B molecule. A detailed investigation regarding the reaction-diffusion process of urotropin particles with different masses on the fast blue B-PAA hydrogel sensor was further dynamically filmed (Supplementary video 2). The enlarged optical images for each particle were extracted along with time lapsed, showing that the particle was gradually solved in hydrogel and lost its crystalline morphology (Fig. S9a). After deducting the background of the hydrogel sensor itself, the coloring procedure was more obvious, showing a progressive extending navy blue spot which quit to extend within 120 s (Fig. S9b and S9c). Subsequently, a statistic investigation was performed by analyzing the diffusion area of 44 particulates with a time-lapse period of 120 s (Fig. 4a).

Supplementary material related to this article can be found online at doi:10.1016/j.jhazmat.2022.129263.

The fast blue B-PAA hydrogel sensor could immediately respond to all urotropin particles within 2 s no matter of the difference in size and the minimal observable particle mass was 17.19 ng with a final spot area of 303 μm, illustrating a rapid response with a naked-eye LOD of 17.19 ng. Compared to other detection methods (Table S3), this work has satisfactory sensitivity without sample pretreatment or heating in the detection process of urotropin. According to the pixel number and the length, as well as the urotropin density, the approximate mass of each particulate was calculated, thus, a positive correlation trend between particle mass and the final diffusion spot area was obtained which suggests a semi-quantitative capability (Fig. 4b). It is worthy to note that the ratio between the diameter of the final diffusion area at 120 s and the actual particle size at 0 s varied from 5.00 to 10.73 (Table S4), indicating the observable particulate diameter was increased at least 5.00 times which empowers an enhanced visible response sensitivity. Furthermore, another four particulates were chosen as the test sample (Fig. 4c), their masses were evaluated through the above established positive correlation between diffusion diameter and particle mass (shown as dash lines in Fig. 4b), which were close to their actual size calculated based on the pixel of their diffusion diameter (labelled as hollow symbols in Fig. 4b. These results illustrate that this hydrogel sensor contributes to amplified sensing response and further prompts a semi-quantification capability to analyze single urotropin particle even with an extremely small size. It is evident that this hydrogel sensor is a promising candidate to sensitively detect the floating particulates which also possesses great possibility to be employed for monitoring other trace environmentally hazardous particulates.

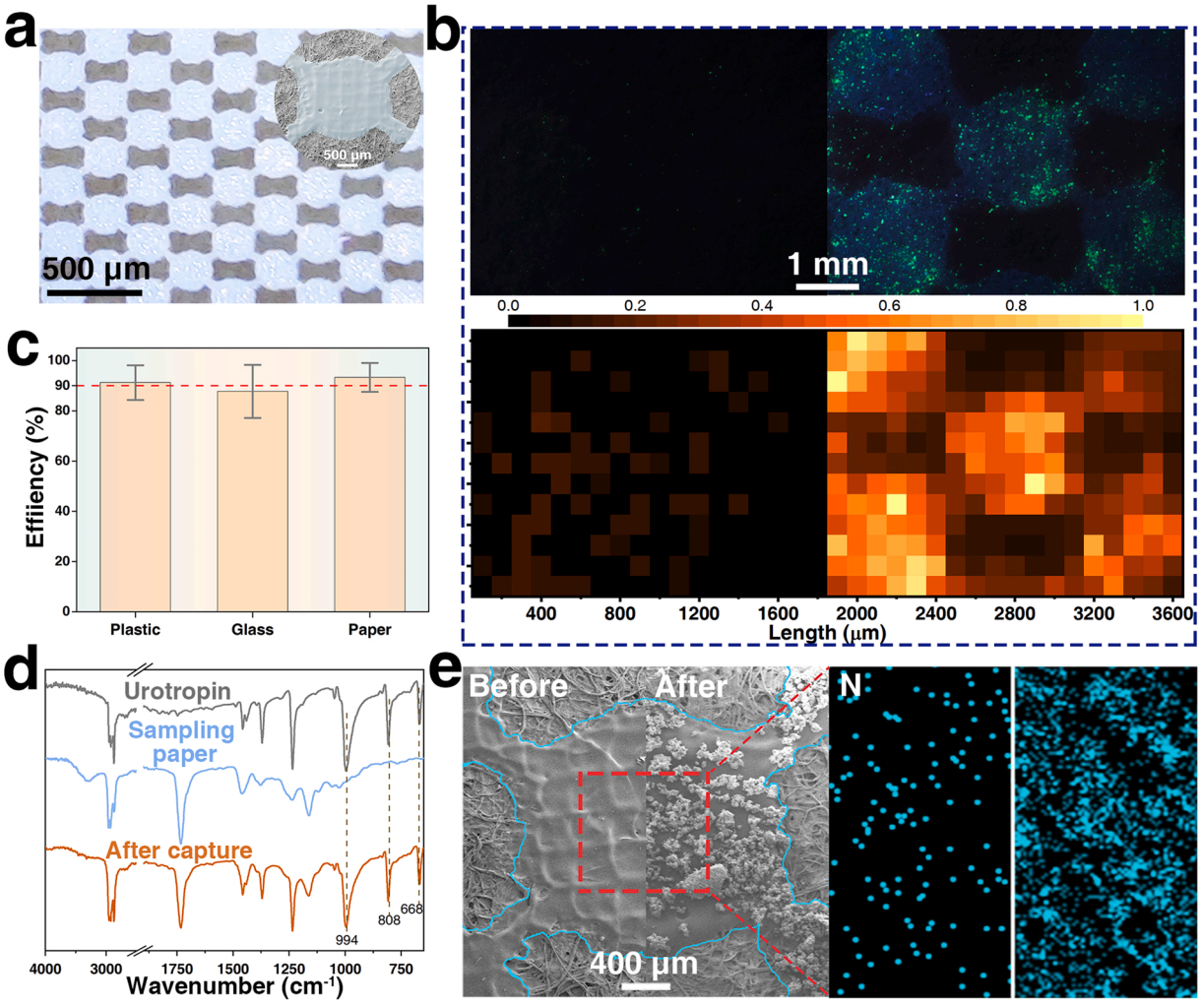

Fig. 5. (a) Photographs of the sampling unit under 365 nm illumination, inset: the amplified SEM image. (b) Photographs of the filter paper (top-left) and sampling unit (top-right) after capturing phosphor particles under 365 nm illumination, and the corresponding heat maps for the fluorescence intensity. (c) Sampling efficiency of the sampling unit towards urotropin particulates on different textures. (d) FT-IR spectra of the sampling unit before and after capturing urotropin particles. (e) Photographs of the morphology of the sampling unit and the N element distribution before and after sampling urotropin particles.

3.5. Construction of the sampling unit and the evaluation on its sampling efficiency

The sampling unit fabricated *via* the screen-printing consists of a paper substrate and a layer of PSAs with the customized pattern, the latter shows slight blue fluorescence under 365 nm UV light (Fig. 5a) with a relatively smooth appearance and sharp edge through the SEM observation (the inset in Fig. 5a). To evaluate the adhere efficiency, both filter paper and the sampling unit were applied to collect the green phosphor powders with gentle touch, subsequently, the comparison images under dark field show that the PSA covered area of the sampling unit exhibits a mass of green dots while very few dots can be found from the filter paper (Fig. 5b). With digitally processing the total intensity of the pixels was calculated as 84.7 for the sampling unit which is 13.2 times higher than that for the filter paper. This well verifies the sampling unit could gather much more particulates with the presence of PSAs, which can be ascribed to the multi-interaction of PSAs towards the subject including hydrogen-bonding, electrostatic interaction, metal complexation and other secondary bonds. To explore whether the object texture would affect the sampling efficiency, 20 mg urotropin powders were placed onto plastic, glass, and paper surface, respectively, after sampling the amount of the remanent powders was examined. It could be seen that whatever the substrate texture was, an excellent sampling performance with the efficiency around 90% was demonstrated (Fig. 5c), and it should also be noted that the PSAs did not remain any residue on the object surface due to its great cohesiveness which could be repeatedly use without warry of the residue issue. FTIR spectroscopy analysis further confirms the sampling result as the distinct characteristic peaks of urotropin (C–N stretching vibration at 994 cm^{-1} and its bending vibration at 808 cm^{-1}/668 cm^{-1}) appear in the spectrum of the sampling unit after sampling (Fig. 5d). Meanwhile, densely stacked urotropin particulates can be observed within the PSAs covered area under SEM after sampling, accompanying plenty of blue dots in energy dispersive spectrometer (EDS) analysis which indicates the N element of urotropin molecule (Fig. 5e). Hence, this PSAs equipped sampling unit exhibits awfully satisfactory sampling efficiency *via* mild action, being conducive to enrich trace particulates and guarantee the prerequisite for highly sensitive detection.

3.6. Expansibility of the sensing chip and the applications in real scenarios

Given that the multi-target detection is imminently expected to cope with the wide-range screening for further assessing environment risk as well as ensuring the operators' health, this pocket sensing chip was obtained by integrating six sensing reagents/probes into the detecting unit with individual partition as a multi-functional tool (Fig. 6a and S10), which could specifically recognize hazardous chemicals, respectively, including perchlorate (Su et al., 2022), potassium permanganate (Liu et al., 2020), urea (Hu et al., 2020), hypochlorite (Jin et al., 2018) and ammonium (Ke et al., 2022; Sasaki et al., 1998). By applying this highly integrated sensing chip to examine the unknown particles on the surface of the mask, the suitcase, the shoe, and the suitcase wheel, it is clearly shown that the detecting array immediately exhibited the characteristic color once it was contacted with the sampling unit (Fig. 6b). It should be noted that even the component or the texture of the sampled surface was rather complicated (*e.g.*, the mask, the shoe, and the zipper) constituting of multi-target or including the environmental interferents (*e.g.*, the wheel), the detection towards the target was not bothered by each other or the non-target particles. Subsequently, the corresponding detecting unit would present the distinguishable coloring (like from light yellow to golden, yellow to violet, colorless to green, yellow to purple-red, colorless to pink and light yellow to olive), warning the existence of the target component (Fig. 6c and Table S5). Furthermore, by digitally extracting the hue value of more than 100 points of each coloring region generated under the experiment condition, a determining range for locating the hue datum of unknown particle was established. Afterwards, a blind test of three points from the measurement towards practical object surface was correctly discriminated based on the above determining range, although the color response of hypochlorite was similar to that of urea by the naked-eye observation, as well as for urotropin and ammonium, which still could be distinguished by the array position. This well illustrates that this sensing chip could be expanded with customized purpose with an outstanding sensing performance to discern multi-target and a great anti-interference capability to external factors, offering a highly effective solution for simultaneously in-field detecting multiple potential hazardous substances.

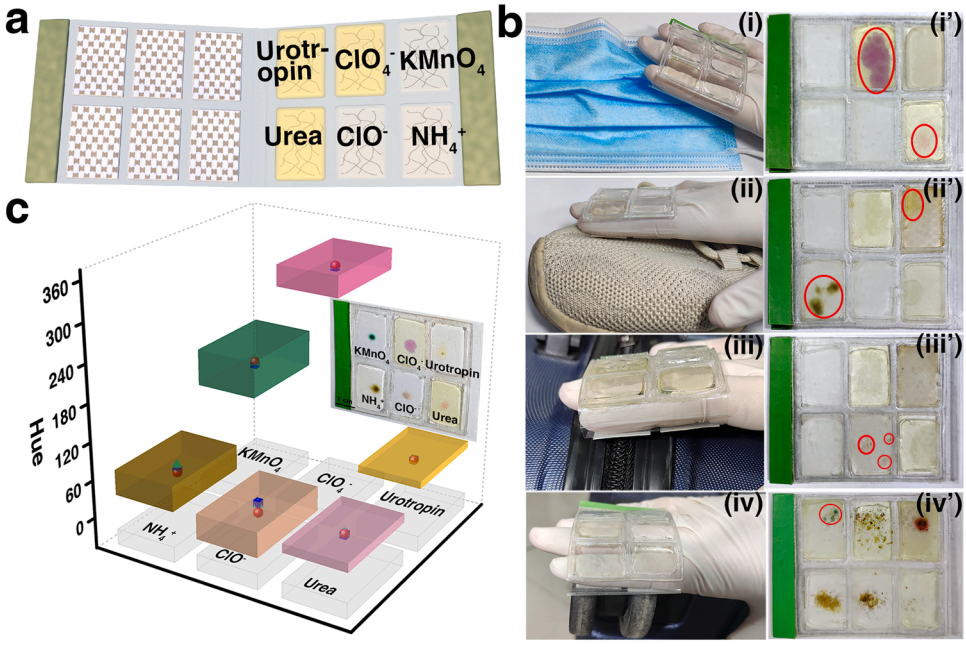

Fig. 6. (a) Schematic illustration of the extended sensing chip with a detecting array. (b) Practical applications for detecting the suspicious particle constituent on the surface of the mask, the shoe, the suitcase, and the wheels. (c) The corresponding coloring responses in detecting 6 hazardous materials and corresponding hue value range of the coloring response in each sensing region, in which the light gray columns represent the location of each sensing region while the columns in different colors stand for the hue value range of each target component after detection, the sphere, cube and tetrahedron were used to represent the hue values of three randomly selected points around the coloring area in Fig. 6b, respectively.

4. Conclusion

In summary, upon the coloring response arising from the electrostatic interaction between urotropin with fast blue B, a unique all-in-one strategy was proposed by integrating the sampling unit and the detection unit as a "pocket sensing chip" to achieve rapid sampling plus directly naked-eye readout within seconds. Specifically, fast blue B holds stronger electropositivity than other diazoniums, empowering a high sensitivity towards urotropin solution (9 μM) as well as great anti-interference capability towards potential co-existing substances under a mild condition. With the loading of fast blue B into the hydrogel, the detecting unit was acquired with an ultra-sensitive and fast response towards urotropin particulates (17.19 ng), while the sampling unit constituted of the pressure-sensitive adhesive with great cohesiveness guaranteed an excellent sampling efficacity of 90% without the residue on the sampled object surface. Moreover, by equipping with multi-sensing reagent/probe, this sensing chip was expanded as a multi-functional tool to be able to recognize multiple targets synchronously in real scenarios, substantially promoting the screening efficacy. We believe that this novel strategy is expected to break through the dilemma of the trace floating hazardous substance particulates, meanwhile, it will open up a perspective for effectively probing multiple critical hazardous chemicals, noxious substances, and even explosives without the concern to the operational safety, maneuverability and portability being confronted by the on-site environmental sensing development nowadays.

CRediT authorship contribution statement

Wenfei Ren: Formal analysis, Methodology, Software, Investigation, Writing – original draft. **Yuan Liu:** Supervision, Investigation, Writing – review & editing. **Baiyi Zu:** Supervision, Methodology, Investigation, Writing – original draft, Writing – review & editing. **Jiguang Li:** Software, Drawing. **Da Lei:** Software, Drawing, Writing – review & editing. **Tianshi Zhang:** Investigation. **Xincun Dou:** Conceptualization, Investigation, Writing – review & editing.

Declaration of Competing Interest

The authors declare that they have no known competing financial interests or personal relationships that could have appeared to influence the work reported in this paper.

Acknowledgment

This work is financially supported by the funders of Natural Science Foundation of Xinjiang (2021D01D04), National Natural Science Foundation of China (21974150, U1903306), Youth Innovation Promotion Association, CAS (No. 2018474), Key Research Program of Frontier Sciences (CAS Grant No. ZDBS-LY-JSC029), and West Light Foundation of the Chinese Academy of Sciences (CAS Grant No. 2020-XBQNXZ-022).

Environmental Implication

Urotropin is widely applied in industry, however, its trace leakage and pollution in aquatic/atmospheric environment could cause asthma and skin irritation, for which it is strictly limited with a threshold value (3.0 mg/m^3) for occupational exposure. Furthermore, it is also used in high explosive manufacturing because of its readily availability (*e.g.*, cyclonite, RDX, a powerful weapon in perpetrating terrorist attack). It is greatly significant to realize ultrasensitive on-site detection of urotropin. This work proposed an integrated all-in-one strategy upon precise molecular modulation to realize an ultrasensitive (17.19 ng), rapid response (2 s) towards single urotropin particulate through a pocket-size chip.

Appendix A. Supporting information

Supplementary data associated with this article can be found in the online version at doi:10.1016/j.jhazmat.2022.129263.

References

Balasubramanian, M., Thennarasu, S., Sudhakaran, T., Perumal, P.T., 2003. Spectrophotometric and fluorimetric determination of hexamine in pure form and its pharmaceutical formulation. Biol. Pharm. Bull. 26, 1211–1214. https://doi.org/10.1248/bpb.26.1211.

Bordin, D.C., Messias, M., Lanaro, R., Cazenave, S.O.S., Costa, J.L., 2012. Forensic analysis: evaluation of interfering vegetable drugs in colorimetric tests for identifying marijuana cannabinoids (Cannabis sativa L.). Quim. Nova 35, 2040–2043. https://doi.org/10.1590/s0100-40422012001000025.

Cai, Y., Wu, Y., Xuan, T., Guo, X., Wen, Y., Yang, H., 2018. Core–Shell Au@metal–organic frameworks for promoting raman detection sensitivity of methenamine. ACS Appl. Mater. Interfaces 10, 15412–15417. https://doi.org/10.1021/acsami.8b01765.

Dubnikova, F., Kosloff, R., Almog, J., Zeiri, Y., Boese, R., Itzhaky, H., Alt, A., Keinan, E., 2005. Decomposition of triacetone triperoxide is an entropic explosion. J. Am. Chem. Soc. 127, 1146–1159. https://doi.org/10.1021/ja0464903.

Forbes, T.P., Krauss, S.T., Gillen, G., 2020. Trace detection and chemical analysis of homemade fuel-oxidizer mixture explosives: emerging challenges and perspectives. TrAC Trends Anal. Chem. 131, 116023 https://doi.org/10.1016/j.trac.2020.116023.

Frisch, M.J., Trucks, G.W., Schlegel, H.B., Scuseria, G.E., Robb, M.A., Cheeseman, J.R., Scalmani, G., Barone, V., Petersson, G.A., Nakatsuji, H., et al. (2016). Gaussian 09, Revision A.02 (Wallingford, CT).

Germain, M.E., Knapp, M.J., 2009. Optical explosives detection: from color changes to fluorescence turn-on. Chem. Soc. Rev. 38, 2543–2555. https://doi.org/10.1039/B809631G.

Grimme, S., Ehrlich, S., Goerigk, L., 2011. Effect of the damping function in dispersion corrected density functional theory. J. Comput. Chem. 32, 1456–1465. https://doi.org/10.1002/jcc.21759.

Gupta, M.K., Mittal, A.K., 2016. Integrated biological and advanced oxidation based treatment of hexamine bearing wastewater: Effect of cow-dung as a co-substrate. J. Hazard. Mater. 308, 394–401. https://doi.org/10.1016/j.jhazmat.2016.01.072.

Hu, X., Ma, Z., Li, J., Cai, Z., Li, Y., Zu, B., Dou, X., 2020. Superior water anchoring hydrogel validated by colorimetric sensing. Mater. Horiz. 7, 3250–3257. https://doi.org/10.1039/D0MH01383H.

Humphrey, W., Dalke, A., Schulten, K., 1996. VMD: visual molecular dynamics. J. Mol. Graph. 14, 33–38. https://doi.org/10.1016/0263-7855(96)00018-5.

Jin, L., Xu, M., Jiang, H., Wang, W., Wang, Q., 2018. A simple fluorescein derived colorimetric and fluorescent 'off–on' sensor for the detection of hypochlorite. Anal. Methods 10, 4562–4569. https://doi.org/10.1039/C8AY01489B.

Jing, X., Mi, H.Y., Peng, X.F., Turng, L.S., 2018. Biocompatible, self-healing, highly stretchable polyacrylic acid/reduced graphene oxide nanocomposite hydrogel sensors via mussel-inspired chemistry. Carbon 136, 63–72. https://doi.org/10.1016/j.carbon.2018.04.065.

Kanter, S.L., Hollister, L.E., Musumeci, M., 1982. Marijuana metabolites in urine of man: X. identification of marijuana use by detection of Δ9-tetrahydrocannabinol-11-OIC acid using thin-layer chromatography. J. Chromatogr. A 234, 201–208. https://doi.org/10.1016/S0021-9673(00)81793-8.

Ke, Y., Liu, Y., Zu, B., Lei, D., Wang, G., Li, J., Ren, W., Dou, X., 2022. Electronic tuning in reaction-based fluorescent sensing for instantaneous and ultrasensitive visualization of ethylenediamine. Angew. Chem. Int. Ed. https://doi.org/10.1002/anie.202203358.

Lee, J.Y., Root, H.D., Ali, R., An, W., Lynch, V.M., Bähring, S., Kim, I.S., Sessler, J.L., Park, J.S., 2020. Ratiometric turn-on fluorophore displacement ensembles for nitroaromatic explosives detection. J. Am. Chem. Soc. 142, 19579–19587. https://doi.org/10.1021/jacs.0c08106.

Lefebvre, C., Rubez, G., Khartabil, H., Boisson, J.-C., Contreras-García, J., Hénon, E., 2017. Accurately extracting the signature of intermolecular interactions present in the NCI plot of the reduced density gradient versus electron density. Phys. Chem. Chem. Phys. 19, 17928–17936. https://doi.org/10.1039/C7CP02110K.

Li, Y., Ma, Y., Jiao, X., Li, T., Lv, Z., Yang, C.J., Zhang, X., Wen, Y., 2019. Control of capillary behavior through target-responsive hydrogel permeability alteration for sensitive visual quantitative detection. Nat. Commun. 10, 1036. https://doi.org/10.1038/s41467-019-08952-1.

Lim, S.H., Feng, L., Kemling, J.W., Musto, C.J., Suslick, K.S., 2009. An optoelectronic nose for the detection of toxic gases. Nat. Chem. 1, 562–567. https://doi.org/10.1038/nchem.360.

Lin, Y., Sun, J., Tang, M., Zhang, G., Yu, L., Zhao, X., Ai, R., Yu, H., Shao, B., He, Y., 2021. Synergistic recognition-triggered charge transfer enables rapid visual colorimetric detection of fentanyl. Anal. Chem. 93, 6544–6550. https://doi.org/10.1021/acs.analchem.1c00723.

Liu, K., Shang, C., Wang, Z., Qi, Y., Miao, R., Liu, K., Liu, T., Fang, Y., 2018. Non-contact identification and differentiation of illicit drugs using fluorescent films. Nat. Commun. 9, 1695. https://doi.org/10.1038/s41467-018-04119-6.

Liu, Y., Li, J., Wang, G., Zu, B., Dou, X., 2020. One-step instantaneous detection of multiple military and improvised explosives facilitated by colorimetric reagent design. Anal. Chem. 92, 13980–13988. https://doi.org/10.1021/acs.analchem.0c02893.

Lock, C.M., Brust, H., van Breukelen, M., Dalmolen, J., Koeberg, M., Stoker, D.A., 2012. Investigation of isotopic linkages between precursor materials and the improvised high explosive product hexamethylene triperoxide diamine. Anal. Chem. 84, 4984–4992. https://doi.org/10.1021/ac300642c.

Louf, J.-F., Lu Nancy, B., O'Connell Margaret, G., Cho, H.J., Datta Sujit, S., 2021. Under pressure: hydrogel swelling in a granular medium. Sci. Adv. 7, eabd2711. https://doi.org/10.1126/sciadv.abd2711.

Lu, T., Chen, F., 2012a. Quantitative analysis of molecular surface based on improved marching tetrahedra algorithm. J. Mol. Graph. Model. 38, 314–323. https://doi.org/10.1016/j.jmgm.2012.07.004.

Lu, T., Chen, F.W., 2012b. Multiwfn: a multifunctional wavefunction analyzer. J. Comput. Chem. 33, 580–592. https://doi.org/10.1002/jcc.22885.

Matzeu, G., Mogas-Soldevila, L., Li, W., Naidu, A., Turner, T.H., Gu, R., Blumeris, P.R., Song, P., Pascal, D.G., Guidetti, G., et al., 2020. Large-scale patterning of reactive surfaces for wearable and environmentally deployable sensors. Adv. Mater. 32, 2001258 https://doi.org/10.1002/adma.202001258.

Miertus, S., Scrocco, E., Tomasi, J., 1981. Electrostatic interaction of A solute with A continuum - a direct utilization of abinitio molecular potentials for the prevision of solvent effects. Chem. Phys. 55, 117–129. https://doi.org/10.1016/0301-0104(81)85090-2.

Murray, J.S., and Politzer, P. (1998). Electrostatic Potentials: Chemical Applications. In Encyclopedia of Computational Chemistry.

Musher, D.M., Griffith, D.P., 1974. Generation of formaldehyde from methenamine: effect of pH and concentration, and antibacterial effect. Antimicrob. Agents Chemother. 6, 708. https://doi.org/10.1128/AAC.6.6.708.

Parker, T.M., Burns, L.A., Parrish, R.M., Ryno, A.G., Sherrill, C.D., 2014. Levels of symmetry adapted perturbation theory (SAPT). I. Efficiency and performance for interaction energies. J. Chem. Phys. 140, 094106 https://doi.org/10.1063/1.4867135.

Parrish, R.M., Burns, L.A., Smith, D.G.A., Simmonett, A.C., DePrince, A.E., Hohenstein, E.G., Bozkaya, U., Sokolov, A.Y., Di Remigio, R., Richard, R.M., et al., 2017. Psi4 1.1: an open-source electronic structure program emphasizing automation, advanced libraries, and interoperability. J. Chem. Theory Comput. 13, 3185–3197. https://doi.org/10.1021/acs.jctc.7b00174.

Pascualahuir, J.L., Silla, E., Tunon, I., 1994. Gepol - an improved description of molecular-surfaces.3. A new algorithm for the computation of a solvent-excluding surface. J. Comput. Chem. 15, 1127–1138. https://doi.org/10.1002/jcc.540151009.

Sasaki, S., Ando, Y., Dejima, M., Arikawa, Y., Karube, I., 1998. A fluorescence-based sensor for ammonium and nitrate. Anal. Lett. 31, 555–567.

Scalmani, G., Frisch, M.J., Mennucci, B., Tomasi, J., Cammi, R., Barone, V., 2006. Geometries and properties of excited states in the gas phase and in solution: theory and application of a time-dependent density functional theory polarizable continuum model. J. Chem. Phys. 124, 094107 https://doi.org/10.1063/1.2173258.

Staymates, J.L., Staymates, M.E., Lawrence, J., 2016. The effect of reusing wipes for particle collection. Int. J. Ion.-. Mobil. Spectrom. 19, 41–49. https://doi.org/10.1007/s12127-015-0185-9.

Stephens, P.J., Devlin, F.J., Chabalowski, C.F., Frisch, M.J., 1994. Ab-initio calculation of vibrational absorption and circular-dichroism spectra using density-functional force-fields. J. Phys. Chem. 98, 11623–11627. https://doi.org/10.1021/j100096a001.

Su, Z., Li, Y., Li, J., Dou, X., 2021. Ultrasensitive luminescent turn-on detection of perchlorate particulates by triggering supramolecular self-assembly of platinum(II) complex in hydrogel matrix. Sens. Actuators B: Chem. 336, 129728 https://doi.org/10.1016/j.snb.2021.129728.

Su, Z., Li, Y., Li, J., Li, K., Dou, X., 2022. Ultrasensitive dual-mode visualization of perchlorate in water, soil and air boosted by close and stable Pt-Pt packing endowed low-energy absorption and emission. J. Mater. Chem. A. https://doi.org/10.1039/D2TA00843B.

Taghdiri, M., Saadatjou, N., Zamani, N., Farrokhi, R., 2013. Heterogeneous degradation of precipitated hexamine from wastewater by catalytic function of silicotungstic acid in the presence of H2O2 and H2O2/Fe2+. J. Hazard. Mater. 246–247, 206–212. https://doi.org/10.1016/j.jhazmat.2012.12.029.

Tan, H., Park, S.-Y., 2021. Poly(acrylic acid) hydrogel microspheres for a metal-ion sensor. ACS Sens. 6, 1039–1048. https://doi.org/10.1021/acssensors.0c02269.

Tininis, A.G., Leandro, A., Pezza, H.R., Melios, C.B., Pezza, L., 2000. Rapid Spot Test Analysis for the Detection of Urotropine in Pharmaceutical Preparations. Anal. Lett. 33, 2901–2912. https://doi.org/10.1080/00032710008543229.

Torphy, T.J., 1994. β-Adrenoceptors, cAMP and Airway Smooth Muscle Relaxation: Challenges to the Dogma. Trends Pharmacol. Sci. 15, 370–374. https://doi.org/10.1016/0165-6147(94)90157-0.

Wang, G., Cai, Z., Dou, X., 2021. Colorimetric Logic Design for Rapid and Precise Discrimination of Nitrate-based Improvised Explosives. Cell Rep. Phys. Sci. 2, 100317 https://doi.org/10.1016/j.xcrp.2020.100317.

Wang, G., Li, Y., Cai, Z., Dou, X., 2020a. A Colorimetric Artificial Olfactory System for Airborne Improvised Explosive Identification. Adv. Mater. 32, 1907043 https://doi.org/10.1002/adma.201907043.

Wang, J., Koo, K.M., Wang, Y., Trau, M., 2018. "Mix-to-Go" silver colloidal strategy for prostate cancer molecular profiling and risk prediction. Anal. Chem. 90, 12698–12705. https://doi.org/10.1021/acs.analchem.8b02959.

Wang, P., Cai, Z., Li, J., Li, Y., Zu, B., Dou, X., 2020b. Dimension confinement effect boosted ultrasensitive colorimetric signal concentrating. Adv. Opt. Mater. 8, 2000524 https://doi.org/10.1002/adom.202000524.

Weigend, F., 2006. Accurate coulomb-fitting basis sets for H to Rn. Phys. Chem. Chem. Phys. 8, 1057–1065. https://doi.org/10.1039/b515623h.

Weigend, F., Ahlrichs, R., 2005. Balanced basis sets of split valence, triple zeta valence and quadruple zeta valence quality for H to Rn: design and assessment of accuracy. Phys. Chem. Chem. Phys. 7, 3297–3305. https://doi.org/10.1039/B508541A.

Xu, X., Duhoranimana, E., Zhang, X., 2017. Selective extraction of methenamine from chicken eggs using molecularly imprinted polymers and LC-MS/MS confirmation. Food Control 73, 265–272. https://doi.org/10.1016/j.foodcont.2016.08.013.

Xu, Y., Wang, H., Luan, C., Fu, F., Chen, B., Liu, H., Zhao, Y., 2018. Porous hydrogel encapsulated photonic barcodes for multiplex microRNA quantification. Adv. Funct. Mater. 28, 1704458 https://doi.org/10.1002/adfm.201704458.

Yanai, T., Tew, D.P., Handy, N.C., 2004. A new hybrid exchange–correlation functional using the coulomb-attenuating method (CAM-B3LYP). Chem. Phys. Lett. 393, 51–57. https://doi.org/10.1016/j.cplett.2004.06.011.

Yi, W., Cai, C., 2008. Synthesis of RDX by nitrolysis of hexamethylenetetramine in fluorous media. J. Hazard. Mater. 150, 839–842. https://doi.org/10.1016/j.jhazmat.2007.10.040.

Zhang, C.X., Du, L.M., 2017. Determination of urotropine using cucurbit 7 uril-palmatine complex as a highly sensitive fluorescent probe. Indian J. Chem. Sect. a-Inorg. Bio-Inorg. Phys. Theor. Anal. Chem. 56, 1161–1165.

Zheng, P., Cui, Z., Liu, H., Cao, W., Li, F., Zhang, M., 2021. Ultrafast-response, highly-sensitive and recyclable colorimetric/fluorometric dual-channel chemical warfare agent probes. J. Hazard. Mater. 415, 125619 https://doi.org/10.1016/j.jhazmat.2021.125619.